Geochemistry Geophysics Geosystems G3
AN ELECTRONIC JOURNAL OF THE EARTH SCIENCES
Published by AGU and the Geochemical Society

Technical Brief
Volume 8, Number 6
29 June 2007
Q06017, doi:10.1029/2007GC001643
ISSN: 1525-2027

Click Here for Full Article

National Geophysical Data Center candidate for the World Digital Magnetic Anomaly Map

S. Maus and T. Sazonova
CIRES at the University of Colorado and NOAA's National Geophysical Data Center, 325 Broadway, Boulder, Colorado 80305-3328, USA (stefan.maus@noaa.gov)

K. Hemant
Goddard Space Flight Center, Greenbelt, Maryland 20770, USA

J. D. Fairhead
GETECH, University of Leeds, LS2 9JT Leeds, UK

Dhananjay Ravat
Department of Geology, Southern Illinois University, Mail Stop 4324, Carbondale, Illinois 62901, USA

[1] Marine and airborne magnetic anomaly data have been collected for more than half a century, providing global coverage of the Earth. Furthermore, the German CHAMP satellite is providing increasingly accurate information on large-scale magnetic anomalies. The World Digital Magnetic Anomaly Map project is an international effort to integrate all available near-surface and satellite magnetic anomaly data into a global map database. Teams of researchers were invited to produce candidate maps using a common pool of data sets. Here we present the National Geophysical Data Center (NGDC) candidate. To produce a homogeneous map, the near-surface data were first line-leveled and then merged by Least Squares Collocation. Long wavelengths were found to agree surprisingly well with independent satellite information. This validates our final processing step of merging the short-wavelength part of the near-surface data with long-wavelength satellite magnetic anomalies.

Components: 5515 words, 5 figures, 1 table.

Keywords: geomagnetic field; crustal field; satellite geomagnetism; aeromagnetic survey; marine magnetic data.

Index Terms: 1545 Geomagnetism and Paleomagnetism: Spatial variations: all harmonics and anomalies; 1541 Geomagnetism and Paleomagnetism: Satellite magnetics: main field, crustal field, external field; 1532 Geomagnetism and Paleomagnetism: Reference fields: regional, global.

Received 23 March 2007; **Accepted** 12 April 2007; **Published** 29 June 2007.

Maus, S., T. Sazonova, K. Hemant, J. D. Fairhead, and D. Ravat (2007), National Geophysical Data Center candidate for the World Digital Magnetic Anomaly Map, *Geochem. Geophys. Geosyst.*, *8*, Q06017, doi:10.1029/2007GC001643.

1. Introduction

[2] Magnetic anomaly maps derived from ship and airborne surveys have played a key role in developing the theory of plate tectonics [*Wegener*, 1912; *Vine and Matthews*, 1963] and unraveling the structure of the Earth's lithosphere [*Phillips et al.*, 1991]. Stitching together large numbers of surveys,

Copyright 2007 by the American Geophysical Union

magnetic anomaly maps have been produced for all of the continents [*Fairhead et al.*, 1997; *Minty et al.*, 2003]. Furthermore, a large marine magnetic track line database is being maintained at the National Geophysical Data Center (http://www.ngdc.noaa.gov/mgg/geodas/trackline.html).

[3] These marine track line data provide a reasonably dense coverage of ocean areas, although sparse data in parts of the southern oceans remain a serious limitation for global mapping.

[4] A key issue in producing a global map is the control of the longest wavelengths [*Ravat et al.*, 2002]. Magnetic anomalies with wavelengths of more than a few hundred kilometers are not reliably determined by stitching together near-surface airborne and marine data. Only satellites can provide the global perspective. The POGO (1967–1971) and Magsat (1979–1980) missions proved that the lithospheric magnetic field is indeed discernible at satellite altitude. However, due to high noise levels and eccentric orbits, lithospheric field models derived from the early satellite data by different techniques disagreed considerably [*Cain et al.*, 1989; *Ravat et al.*, 1995; *Cohen and Achache*, 1990]. A breakthrough was achieved with the CHAMP satellite [*Reigber et al.*, 2002], launched in July 2000. With its high-accuracy instrumentation and long life at low orbital altitudes, CHAMP has made it possible for the first time to accurately map large-scale magnetic anomalies in the 400 km to 2500 km waveband [*Maus et al.*, 2002, 2007]. Indeed, with CHAMP operating at continuously decreasing altitude, resolution may improve to 300 km in coming years. This information on the long wavelength field is essential for integrating regional data into a global anomaly map.

[5] The final step of producing such a global magnetic anomaly map is only now being undertaken in a concerted effort, lead by a task force of the International Association for Geomagnetism and Aeronomy (http://www.ngdc.noaa.gov/IAGA/vmod/). The aim of this effort is to produce a World Digital Magnetic Anomaly Map (WDMAM). The task force has asked all organizations holding marine and aeromagnetic data to contribute track line data and 5 km resolution grids to the WDMAM project. This call for data has been encouragingly successful, with good coverage of near-surface data now available for the first version of the WDMAM, to be unveiled at the International Union for Geophysics and Geodesy (IUGG) General Assembly in Perugia, Italy, in July 2007. In order to arrive at a high-quality scientific product, a call for candidate models for WDMAM was issued in June 2006, and six candidates were submitted to the task force in November 2006 for evaluation. The candidate models were produced by teams at the Geological Survey of Finland (GTK), NASA, University of Leeds, GeoForschungszentrum Potsdam (GFZ), and NGDC. Following evaluations by internal and external reviewers, the NGDC candidate was selected by the WDMAM task force as a base map, to undergo further modifications by the other teams. The resulting community map will be distributed as the official WDMAM in print and digital form by the Commission for the Geological Map of the World. This paper describes the NGDC candidate, produced by the authors of this paper.

2. Methods

[6] The guiding principles for our processing methodology were (1) to provide the most accurate estimate of the lithospheric magnetic field on the final grid and (2) to produce a homogeneous grid whose horizontal derivatives were dominated by geological features rather than by data artifacts. In implementing the second goal, we accepted that the resulting product would be somewhat smoother than the actual lithospheric magnetic field. Two methods were used here which require further explanation. The first is a Least Squares Collocation method [*Moritz*, 1980] which we used to generate a grid from arbitrarily located input measurements. The second is a line-leveling method [*Paterson and Reeves*, 1985] used to correct for random offsets between track lines.

2.1. Least Squares Collocation

[7] The WDMAM grid is defined as the magnetic field anomaly at an altitude of 5 km above the WGS84 reference ellipsoid with an angular resolution of 3 arc minutes. Future versions of the WDMAM may be defined at a higher resolution and lower altitude. Since the locations of the given measurements are usually not identical to the WDMAM grid nodes, one requires a procedure to estimate the field at those nodes. In principle, there appear to be at least two ways of achieving this. The first is to use a Fourier method. However, a Fourier approach assumes plane geometry, can produce edge effects, cannot handle track line data, has to be specifically adapted to draped surveys (varying survey altitude), and cannot simultaneously handle several data sets. Instead, we

therefore used Least Squares Collocation (LSC), a popular method in geodesy [*Moritz*, 1980]. With the LSC method one can directly estimate the magnetic field at a desired location and altitude, taking into account all neighboring magnetic field measurements. The use of LSC for magnetic field studies is described well in the book of Chapter 5.3.3 *Langel and Hinze* [1998] and can be summarized as follows:

[8] The goal is to estimate a vector of magnetic anomaly field values b at a number of different locations, given a vector of magnetic anomaly measurements c at surrounding locations with possibly different altitudes. The measurement vector can be thought of as the sum of the true anomaly vector a plus an error vector e. One has to take into account the horizontal and vertical separation of the measurements from the locations at which b is to be estimated. For this purpose, one makes a statistical assumption on how the field behaves with horizontal and vertical separation. *Langel and Hinze* [1998, chap. 5.3.3, p. 137] propose two correlation functions which they call V_2 and V_3. The model correlation functions V_2 and V_3 are given by

$$V_2(\delta_{1,2}, z_1, z_2) = V_0\beta\left(\delta_{1,2}^2 + (z_1 + z_2 + \beta)^2\right)^{-1/2},$$

$$\beta = r_c/\sqrt{3} \tag{1}$$

$$V_3(\delta_{1,2}, z_1, z_2) = V_0\beta^2(z_1 + z_2 + \beta) \cdot \left(\delta_{1,2}^2 + (z_1 + z_2 + \beta)^2\right)^{-3/2},$$

$$\beta = r_c/0.766 \tag{2}$$

where $\delta_{1,2}$ is the horizontal separation and z_1 and z_2 are the vertical coordinates of two locations 1 and 2. Both correlation functions have two free parameters, the variance V_0 and the correlation length r_c. The parameter V_0 is just a linear scale factor for the y axis, while r_c can be interpreted as a scale factor on the x axis. Scaling along the x axis is further influenced by the altitude of the measurement and grid locations, reflecting the fact that a larger correlation length of the sources and a larger vertical distance to the sources both lead to a smoother field.

[9] The correlation function V_3 falls off more rapidly with distance than V_2. Since magnetic anomaly fields are generally less smooth than gravity fields, it seemed likely that the function V_3 would turn out to be more suitable for magnetic anomaly modeling, which was confirmed in the following analysis. To verify the suitability of V_2 and V_3 and to estimate V_0 and r_c, we computed the empirical correlation functions for some arbitrarily chosen rectangular areas in the NGDC magnetic grid of the former Soviet Union, the Australian and the North American magnetic anomaly grids (see Table 1). The correlation functions are displayed in Figure 1. We find that V_3 gives a better fit than V_2. By trial and error, we infer values of V_0 = 40,000 nT^2 and r_c = 15 km which are used for all locations.

[10] The least squares estimate $\underline{\mathbf{b}}$ of the vector of anomalies $\mathbf{b}$ is then given by

$$\underline{\mathbf{b}} = V_{a,b}^T V_c^{-1}\mathbf{c} \tag{3}$$

where the matrix $V_{a,b}$ is defined as

$$V_{a,b} = V_3(\delta_{a,b}, z_a, z_b), \tag{4}$$

evaluated for all pairs of estimation (b) and measurement (a) locations [*Langel and Hinze*, 1998, p. 136]. Correspondingly, the matrix V_c is given by

$$V_c = E(\mathbf{e}\mathbf{e}^T) + V_3(\delta_{1,2}, z_1, z_2) \tag{5}$$

evaluated for all pairs of measurements. Here, $E(\mathbf{e}\mathbf{e}^T)$ is the expected error co-variance matrix. The beauty of this term is that it allows to specify correlated errors for data within the same data set. Such correlated errors are due to systematic offsets between neighboring tracks, or between a track and a grid. In fact, such offsets are the dominant uncertainties in the data. We assumed that (after line leveling) the uncorrected offset is 25 nT, and that this is the primary source of error. Thus we chose

$$E(\mathbf{e}\mathbf{e}^T) = \begin{cases} 625\ \text{nT}^2 & \text{for data pairs from the same set} \\ 0\ \text{nT}^2 & \text{for data pairs from different sets.} \end{cases} \tag{6}$$

In summary, the LSC method allows for the optimal estimation of a grid from multiple data sets taking into account different survey altitudes and random offsets between data sets.

2.2. Line Leveling of Marine and Airborne Track Line Data

[11] Even under the optimum conditions of a single aeromagnetic survey with ground reference stations, track lines end up having random offsets. In aeromagnetic surveys, these are corrected using

Table 1. Summary of Data Sets, With Their Official WDMAM Codes, Coverage, and References[a]

Code	Area Covered	Res	Reference
701.43	North America	1 km	NAMAG, http://pubs.usgs.gov/sm/mag_map/
302.43	Antarctica	5 km	ADMAP, http://www.geology.ohio-state.edu/geophys/admap/
504.43	Australia	1 km	Geoscience Australia, http://www.ga.gov.au/
601.43	Europe	5 km	Wonik, BGR, http://www.bgr.bund.de/
121.43	Arctic	5 km	GSC, http://gsc.nrcan.gc.ca/index_e.php
421.43	Middle East	1 km	AAIME, http://home.casema.nl/errenwijlens/itc/aaime/
411.43	East Asia	2 km	CCOP, http://www.ccop.or.th/
442.2	India	50 km	*Qureshy* [1982]
441.3	India	5 km	GSI, http://www.gsi.gov.in/
201.2	Africa	15 min	GETECH, http://www.getech.com/
201.2	S. America	15 min	GETECH, http://www.getech.com/
625.2	France	10 km	IPGP, http://www.ipgp.jussieu.fr/
627.43	Spain	1.5 min	*Socias et al.* [1991]
222.3	South Africa	5 km	SADC, http://www.sadc.int/
611.3	Fennoscandia	5 km	GTK, http://www.gtk.fi/
626.2	Italy	5 km	*Chiappini et al.* [2000]
622.2	Canary Islands	5 km	*Socias and Mezcua* [1996]
812.3	Argentina margin	5 km	Ghidella, DNA, http://www.dna.gov.ar/
811.45	Argentina inland	5 km	SEGEMAR, http://www.segemar.gov.ar/db/
401.3	Eurasia	2 km	GSC, http://gsc.nrcan.gc.ca/index_e.php
628.3	Russia	5 km	VSEGEI, http://www.vsegei.ru/WAY/247038/locale/EN
101.45	Marine track line	variable	NGDC, http://www.ngdc.noaa.gov/mgg/geodas/trackline.html
131.45	Project Magnet	variable	NGDC, http://www.ngdc.noaa.gov/seg/geomag/proj_mag.shtml

[a] Some resolutions (Res) are given in arc minutes (min).

perpendicular tie lines [*Paterson and Reeves*, 1985]. The marine track line data used for the WDMAM is much more prone to this kind of error. In addition, the older data may have navigational errors, a problem which is addressed later by rejecting incompatible track segments. The data are measured over a time span of 50 years, sometimes thousands of kilometers away from the nearest magnetic observatory. Apart from incompletely removed main and external fields, there are also likely to be instrument biases. The resulting uncertainty in the longer wavelength part of the magnetic field can be dealt with by line leveling, which minimizes the misfit between neighboring or crossing tracks.

[12] To each track with index i we assign a correction function

$$f_i(d) = \sum_{k=0}^{N_i} a_{i,k} \cos(\pi k d / D_i) \tag{7}$$

where D_i is the great circle distance from the first to the last point of the track and N_i is the number of parameters used for the correction function of the track. We use $N_i = trunc(D_i/400\ \text{km}) + 1$. Thus we roughly assume that all information in the track with a half-wavelength exceeding 400 km is unreliable and is subject to adjustment in the line leveling. In one grand inversion, we then estimated the optimum parameters $a_{i,k}$, which minimize the misfit between all neighboring tracks and simultaneously minimize the misfit of the track line to the gridded data. In this procedure the gridded data are not modified. To account for the distance between

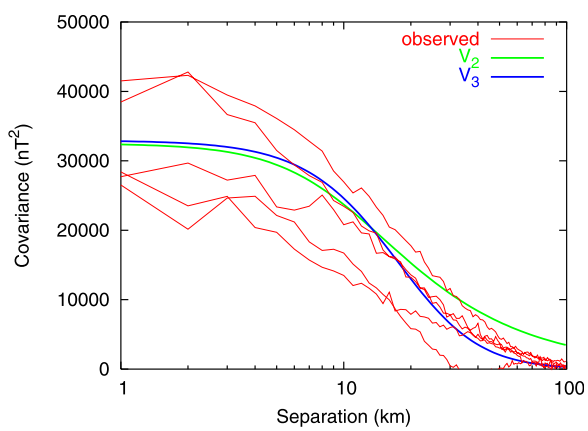

Figure 1. Observed correlation functions, computed from arbitrary rectangular areas in the NGDC magnetic grid of the former Soviet Union and the Australian and the North American magnetic anomaly grids. Overlain are the model correlation functions of equations (1) and (2), assuming a uniform survey altitude of 1000 m. The model V_3 gives a better fit than V_2.

measurement locations in computing the misfit, we use the weight function

$$W(\delta_{1,2}, z_1, z_2) = \max\left(0, 1 - \frac{1}{R_s}\sqrt{(\delta_{1,2}^2 + 2(z_1 - z_2)^2}\right) \tag{8}$$

where R_s = 100 km is the search radius, and $\delta_{1,2}$, z_1 and z_2 are again the horizontal separation and the vertical coordinates, respectively. In this definition of the weight function, the vertical separation is upweighted by a factor 2 in order to account for the greater variability of a poloidal field in the vertical than in the horizontal direction.

3. Input Data

[13] The input data fall into three different categories: (1) marine and aeromagnetic track line data, (2) large-scale aeromagnetic and marine magnetic grids, and (3) CHAMP satellite data which are included in form of the MF5 model [*Maus et al.*, 2007]. The data sets are listed in Table 1.

4. Data Processing Steps

[14] Our data processing scheme starts with combining the existing grids to a single common grid, then preparing the track line data and merging them to a combined grid, and finally replacing the longest wavelengths with MF5.

4.1. Gridded Data

[15] Most aeromagnetic surveys over land have already been combined to country-wide or even continental compilations. These compilations are mostly very well made, and it would be far beyond the scope of the WDMAM project to locate and reprocess individual surveys that contributed to these large-scale compilations.

[16] In some cases, areas are covered by several compilations. If in such cases one of the compilations is known to have superior resolution or accuracy, overlapping parts of the lower quality grids were discarded. This applies to (1) the 50 km resolution ground magnetic survey of India (code 442.2), which is partly covered by the 5 km resolution aeromagnetic map of India (code 441.3), (2) the GSC compilation of Eurasia (code 401.3), which is partly covered by the new Russian grid (code 628.3), and (3) the 15 arc minute GETECH data of South America, Africa and Asia (code 201.2), which are partly covered by various smaller 5 km resolution grids.

[17] In order to avoid the possible loss of information in the following processing steps, we resampled all grids to 1.5 arc minute angular resolution using the minimum curvature algorithm (program "surface") of Generic Mapping Tools (GMT) [*Wessel and Smith*, 1991].

[18] The LSC method takes into account the exact altitude of the measurements. Some compilations are provided at barometric altitude. However, most compilations are draped, meaning that they follow the surface topography at a constant altitude above terrain. For the accurate processing of the altitude information, one therefore requires a topographic model of the Earth. We used NGDC's ETOPO-2 surface elevation grid (http://www.ngdc.noaa.gov/mgg/global/global.html), which we linearly interpolated to the measurement positions and added to the terrain clearance of all draped surveys, in order to compute the measurement altitude above the geoid.

[19] In the merging of the compilations, random offsets between neighboring and overlapping grids must be adjusted. These random offsets reflect inherent uncertainties at long wavelengths, caused by stitching together small-scale surveys. To deal with such edge effects, we first subtracted a linear 2D trend from all smaller size grids. Then we computed the distance to the nearest margin for all points of every grid. Finally, we merged the grids by LSC (see section 2), using weights which are linearly proportional to the distance from the margin, starting at 0.01 on the margin and extending to a maximum value of 1.0 for 200 km inland. This procedure may introduce spurious anomalies with half-wavelengths larger than 200 km. However, these spurious anomalies are largely removed at a later stage, when the long wavelengths are substituted with the MF5 model.

4.2. Track Line Data

[20] Short wavelength noise in marine and aeromagnetic track line data is mostly caused by external fields. Identifying such disturbed sections is a challenging task. In particular, genuine crustal anomalies can exceed strengths of 1000 nT, while external field disturbances with amplitudes of 100 nT already give rise to spurious magnetic anomalies. Thus disturbed sections cannot be identified by residual amplitude. However, ships and aircraft move relatively slowly, while strong external field disturbances change rather rapidly. We therefore used the along-track derivative of the magnetic field residual as a selection criterion. If

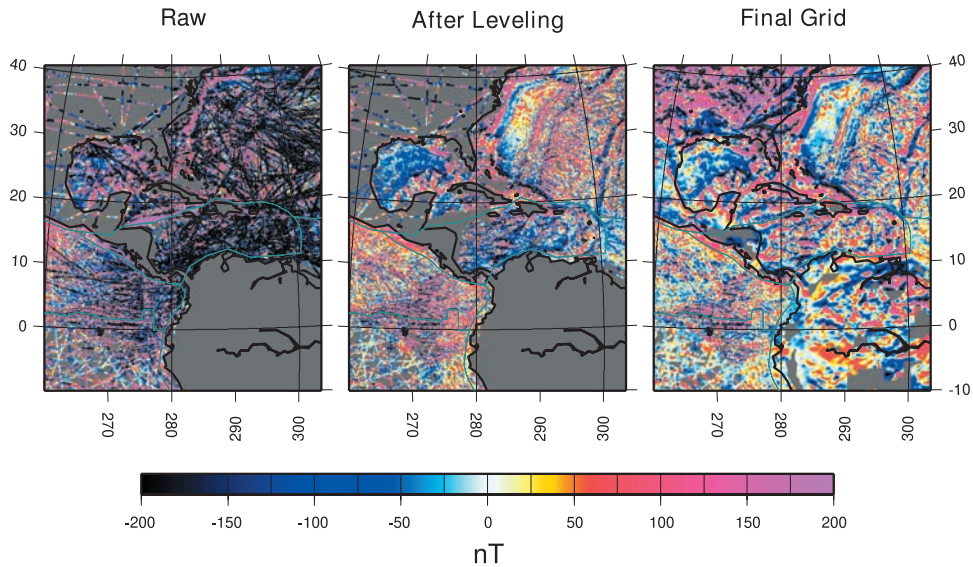

Figure 2. Processing and merging of track line and gridded data, illustrated for Central America. The left panel shows the raw marine and aeromagnetic data. Line leveling and discarding tracks with remaining high offsets lead to the middle panel. Finally, the merger with the gridded data (which also cover parts of the oceans) and the correction of the long wavelengths with the satellite model MF5 lead to the final result shown in the right panel.

the derivative exceeded 100 nT/km, the 20 preceding and following measurement points were discarded. The threshold of 100 nT for the along-track gradient was found by trial and error, using a test area with strong ocean magnetic anomalies in the North Pacific. This threshold eliminated about 3% of the marine track line data and 9% of the Project Magnet data. It is not clear why the Project Magnet data seemed noisier than the marine data. In fact, one may have expected the opposite. This surprising discrepancy in data quality will have to be investigated in the run-up to the next edition of the WDMAM.

[21] In order to reduce the huge volume of data, the track line data were resampled by averaging in 2.5 km bins. For the subsequent line leveling, the data were further broken into straight segments. The NGDC marine data consist of about 20 million points on 28,000 tracks, which we broke into 91,000 segments and resampled to 4 million points. Similarly, 7 million Project Magnet measurements on 3000 tracks were broken up into 7,000 segments and resampled to 800,000 points.

[22] Using the procedure described in section 2, we then line-leveled the 98,000 track segments against each other by estimating 110,000 correction coefficients which simultaneously minimized offsets where tracks overlap with the gridded data. After leveling, plotting the misfits reveals some large outliers of segments which could not be brought into agreement with the other data. This is expected for segments with strong external disturbances or segments with incorrect positions due to navigation errors. After visual inspection of the distribution of misfits, we discarded the segments with a remaining between-segment misfit exceeding 550 nT, or a misfit against the gridded data exceeding 500 nT. This removed about 1% of the segments. The leveling and selection reduced the root-mean-square (rms) between-segment misfit from 380 nT to 130 nT (i.e., 81 nT if only exact cross-overs are counted) and the misfit against the gridded data from 400 nT to 90 nT.

[23] Finally, the leveled line data were merged with the gridded data, again using the LSC method, taking into account the altitude of the ship-borne and Project Magnet data.

[24] An example of the effect of line leveling and the final merge is shown in Figure 2. The left panel shows the raw track line data, the middle shows the leveled and selected data, while the right panel shows the final map after merging with the gridded data and long-wavelength substitution. Several interesting inferences can be made from this figure. The first is that the input data are indeed seriously offset against each other. This is mostly due to the Earth's changing main magnetic field, and the limited accuracy of the reference fields used for the original main field corrections. However, these offsets are of long wavelength and are removed by

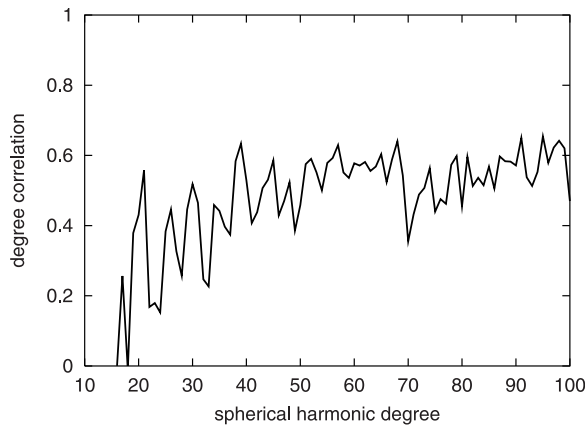

Figure 3. Degree correlation, as defined by equation (9), between the satellite-only model MF5 and our model from the merged near-surface data. Considering the completely different nature of the two data sets, the correlation is surprisingly high.

the line leveling, as seen in the middle panel. A problem in the line leveling is exposed for the Cayman trough, where the track line data of an entire area were rejected because they exceeded the rms threshold. This should probably not have happened and needs to be investigated prior to the next map edition. Fortunately, this omission had only a limited impact on the final map because the area is covered by the North American compilation. Adding the North American compilation introduced new problems, however: Off the Pacific coast of Central America (Figure 2, middle panel) one can see convincing small-scale linear features trending southeast. Unfortunately, these features are strongly suppressed when adding on the North American compilation. This observation also holds in other ocean areas, where line-leveled marine data often provide more accurate information than the compilations, although they were produced largely from the same original measurements.

4.3. Substituting the Longest Wavelengths With a CHAMP Satellite Model

[25] Long wavelengths in grid and track line data are known to be highly inaccurate. This is primarily due to temporal changes of the main field. Stitching together surveys and tracks collected at different times only allows for very limited control of wavelengths exceeding typical survey sizes of a few hundred kilometers. These long wavelengths are more accurately recorded by low-orbiting satellites. Since 2000, the CHAMP satellite has been measuring the magnetic field with unprecedented accuracy. Here, we used the lithospheric field model MF5 [*Maus et al.*, 2007], estimated from the latest three years of CHAMP data from August 2003 through July 2006.

[26] There are several ways to replace the long wavelengths of the combined grid with MF5 in the spectral domain. We chose a processing route via the magnetic potential. A total intensity data coverage on the sphere does not completely constrain the magnetic potential [*Backus*, 1970]. The ambiguity is further increased by the incomplete data coverage. By using the least squares method and eliminating the lowest Eigenvalues, one can select one of many magnetic potentials that represent the observed anomaly. We computed this magnetic potential of the near-surface data to degree 120. Figure 3 shows the degree correlation between this model and MF5. If the coefficients of one model are denoted by g_n^m and the other by k_n^m the correlation as a function of degree n is defined here following *Langel and Hinze* [1998, equation (4.23)] as

$$C(n) = \frac{\sum_m g_n^m k_n^m}{\left[\sum_m \left(g_n^m\right)^2 \sum_m \left(k_n^m\right)^2\right]^{1/2}} \tag{9}$$

Note that the two data sources are completely independent. No satellite data have been used in our grid, neither for the track line data nor the gridded data. In particular, we used the original, unfiltered NAMAG grid, rather than one of its modifications where long wavelengths were substituted with satellite magnetic models. The correlation increases to an encouragingly high value of about 0.6 at degree 100, validating the high-degree coefficients of MF5. Indeed, the high correlation indicates that valuable small-scale signal is contained in the satellite data beyond degree 100. One could even argue that MF5 should have been expanded up to the degree where the correlation peaks before decreasing to zero. We will take note of this when producing the next generation satellite lithospheric model MF6.

[27] Another important check before replacing the long wavelengths with MF5 is to see how well their power spectra agree. Figure 4 shows the near-surface data spectrum in comparison with MF5. The near-surface data exhibit strong low-degree power, caused by unremoved main field in the continental scale grids. At high degrees, however, the power of the near-surface data is only about 10% higher than MF5. Again, considering the different data sources and the multitude of processing steps and corrections, a disagreement of 10% in

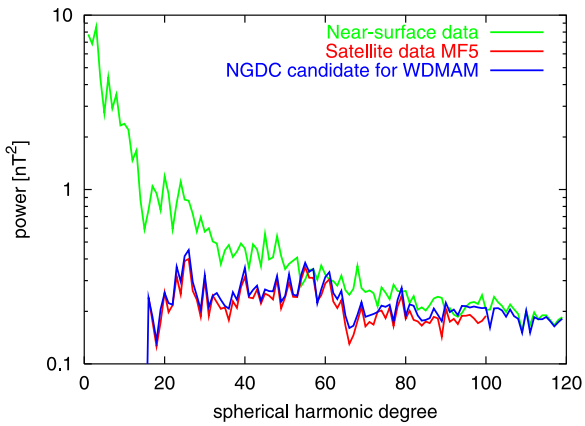

Figure 4. Spectra of the near-surface-data spherical harmonic model and MF5. The high power at low degrees in the near-surface data is primarily due to uncorrected main field. At high degrees, on the other hand, the power levels in the two models differ only by about 10%. The blue line shows the spectrum of the final NGDC candidate map.

power (which amounts to even less in amplitude) is encouragingly small. It is difficult to pin-point the source of this discrepancy which is probably a mix of several effects. The prime candidate for a lack of power in MF5 is the removal of genuine field in the rigorous processing of the satellite data, while excess power in the near-surface data at 400 km wavelength could be due to spurious large-scale features introduced in the stitching together of small-area surveys.

[28] Given the good spectral agreement between MF5 and the near-surface model at degree 100, we use a sharp cut-off to substitute the long wavelengths of the near-surface data with the MF5 model. This substitution was carried out by subtracting the near-surface model to degree 100 from each grid cell and then adding the prediction from MF5.

4.4. GIS Flags

[29] The format definition of the WDMAM grid includes a fourth column identifying the primary data source of each grid cell. This information is of course not unique in areas of overlapping data sets. We decided that gridded data should have priority over track line data, reflecting the line leveling onto the gridded data. As mentioned above, we had discarded areas of the lower-resolution grids which were covered already by higher-resolution grids. In remaining overlap areas, our present flagging is somewhat arbitrary. In future map editions a hierarchy of the different data sets based on data resolution and accuracy should be assigned.

5. Result

[30] The final result (Figure 5) of the processing is a three arc minute angular grid of the total intensity anomaly at 5 km above the WGS84 geoid. In the grid, unsurveyed areas are filled with the satellite-only model MF5 and flagged with code 13. It should be noted, however, that plotting these fill-in values as part of the map can lead to serious misinterpretation since it is then unclear whether the field is smooth because of the geologic setting or because of inadequate data coverage. This problem is particularly obvious in the southern Indian Ocean, where the mid ocean ridge stands out clearly as a positive anomaly. This occurs not because the ridge is particularly magnetic, but because it is the only well-surveyed area in the region. Most likely, there are equally strong parallel patterns, but in the absence of measurements the grid defaults to the smooth MF5 model. Such misinterpretation is avoided if the fill-in values are not plotted as part of the map. We therefore prefer to plot the field only for areas where near-surface data are available. This has the additional advantage of showing where further data are needed for future WDMAM editions, hopefully motivating new data collection efforts.

[31] In plotting the final map (Figure 5), we find that there is a technical difficulty in displaying single track lines. Ideally, the lines should be equally broad for North/South and East/West oriented tracks. However, due to anisotropic stretching in global projections track line widths are distorted. With the Generic Mapping Tool's Mercator projection, North/South oriented tracks become very wide and East/West oriented tracks exceedingly thin. For our final map we therefore used GMT's Mollweide projection, which avoids this distortion. The polar stereographic projections did not exhibit this problem.

6. Grid Availability and Outlook

[32] The official WDMAM is expected to be released in July 2007 at the Meeting of the International Union of Geodesy and Geophysics in Perugia. There will be a paper copy of the map, as well as a DVD with the digital grid and the candidate WDMAM submissions, to be distributed by the Commission for the Geological Map of the World, 77, rue Claude-Bernard, 75005 Paris,

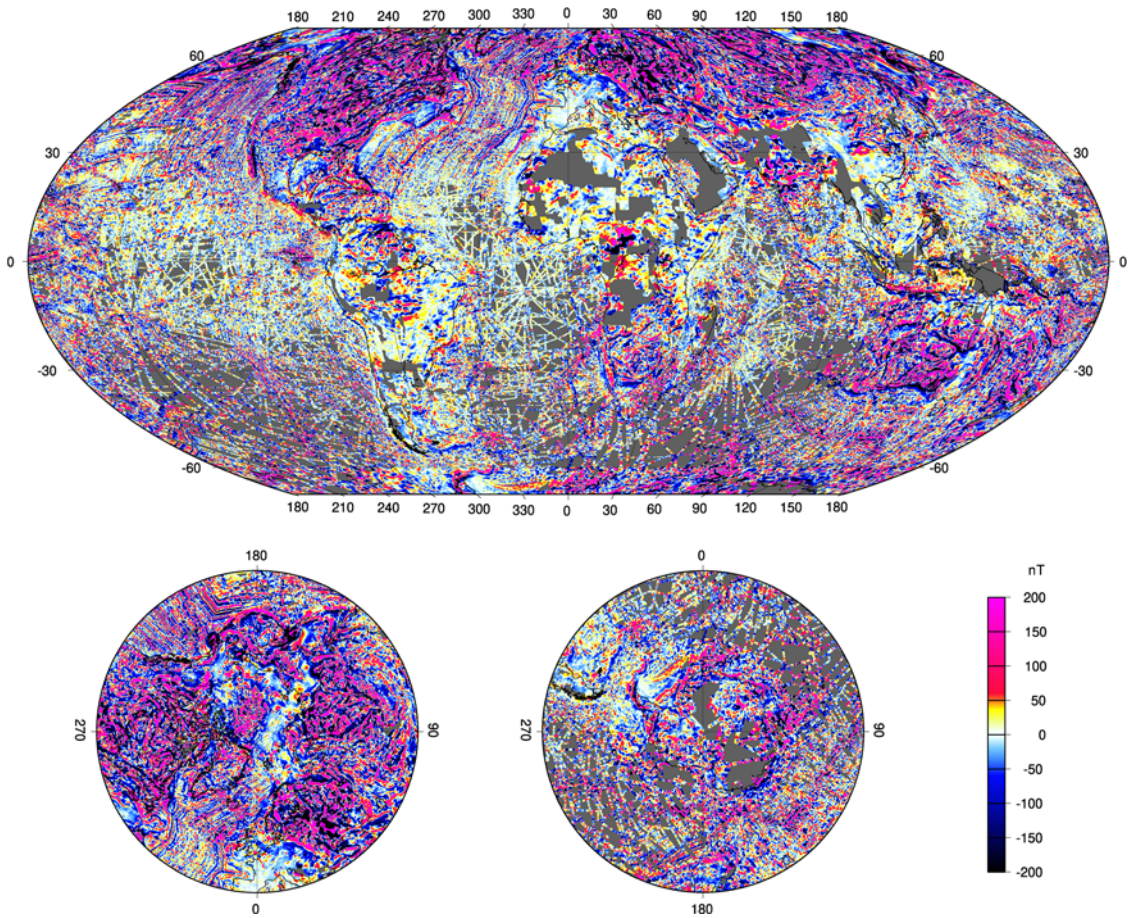

Figure 5. The final NGDC WDMAM candidate grid. The top panel shows a Mollweide projection with cut-off at 70° latitude. The polar stereographic projections in the bottom two panels extend down to 40° in latitude.

France. The digital grid of the NGDC candidate for WDMAM is already publicly available at http://geomag.org/models/wdmam.html and at http://earthref.org/cgi-bin/erda.cgi?n=735 as a permanent archive. Furthermore, a package for visualization of the map in NASA World Wind can be downloaded from http://www.getech.com/downloads/WDMAM.

[33] The WDMAM is an ongoing project, with plans to produce updates of the map and grid every couple of years. As part of these updates, additional data will be acquired for presently uncovered areas. Some of these areas have already been surveyed but the data are not readily accessible, for various reasons. It is our hope that the WDMAM will enjoy widespread usage, creating momentum to conduct further aeromagnetic surveys and help to complete the global coverage.

[34] Further significant improvements in accuracy and resolution can be expected at long wavelengths of the spatial spectrum which is supplied by low-orbiting satellites. The CHAMP mission is expected to continue providing excellent quality data at solar minimum conditions and at steadily decreasing altitudes up to the year 2009. Following in 2010 is the European Space Agency's *Swarm* mission, a constellation comprising 3 satellites (http://www.esa.int/esaLP/LPswarm.html). This will further improve lithospheric magnetic anomaly maps by providing direct measurements of magnetic field gradients [*Maus et al.*, 2006].

[35] Thus a more complete spatial coverage by marine and aeromagnetic data, together with better control of the long wavelengths from new satellite missions, offers the scope for further significant improvements in upcoming WDMAM editions.

Acknowledgments

[36] We thank two referees, Richard Blakely and Erwan Thebault, for numerous suggestions that helped to improve

this manuscript. The organizations listed in Table 1 provided marine and aeromagnetic data for the WDMAM project. We are particularly indebted to Juha Korhonen and other members of the WDMAM task force for their successful negotiations with the various data providers. The work presented in this paper was partly supported by Deutsche Forschungsgemeinschaft in the Special Program "Geomagnetic Variations" (SPP 1097). The operational support of the CHAMP mission by the German Aerospace Center (DLR) and the financial support for the data processing by the Federal Ministry of Education and Research (BMBF) are gratefully acknowledged.

References

Backus, G. E. (1970), Non-uniqueness of the external geomagnetic field determined by surface intensity measurements, *J. Geophys. Res.*, *75*, 6339–6341.

Cain, J. C., Z. Wang, C. Kluth, and D. R. Schmitz (1989), Derivation of a geomagnetic model to n = 63, *Geophys. J. Int.*, *97*, 431–441.

Chiappini, M., A. Meloni, E. Boschi, O. Faggioni, N. Beverini, C. Carmisciano, and I. Marson (2000), On shore-off shore integrated shaded relief magnetic anomaly map at sea level of Italy and surrounding areas, *Ann. Geofis.*, *43*, 983–989.

Cohen, Y., and J. Achache (1990), New global vector magnetic anomaly maps derived from Magsat data, *J. Geophys. Res.*, *95*, 10,783–10,800.

Fairhead, J. D., D. J. Misener, C. M. Green, G. Bainbridge, and S. W. Reford (1997), Large scale compilation of magnetic, gravity and electromagnetic data: The new exploration strategy for the 90's, in *Proceedings of Exploration 97: Fourth Decennial International Conference on Mineral Exploration*, edited by A. G. Gubins, pp. 805–816, GEO F/X, Toronto, Canada.

Langel, R. A., and W. J. Hinze (1998), *The Magnetic Field of the Earth's Lithosphere: The Satellite Perspective*, Cambridge Univ. Press, New York.

Maus, S., M. Rother, R. Holme, H. Lühr, N. Olsen, and V. Haak (2002), First scalar magnetic anomaly map from CHAMP satellite data indicates weak lithospheric field, *Geophys. Res. Lett.*, *29*(14), 1702, doi:10.1029/2001GL013685.

Maus, S., H. Lühr, and M. E. Purucker (2006), Simulation of the high-degree lithospheric field recovery for the swarm constellation of satellites, *Earth Planets Space*, *58*, 397–407.

Maus, S., H. Lühr, M. Rother, K. Hemant, G. Balasis, P. Ritter, and C. Stolle (2007), Fifth-generation lithospheric magnetic field model from CHAMP satellite measurements, *Geochem. Geophys. Geosyst.*, *8*, Q05013, doi:10.1029/2006GC001521.

Minty, B. R. S., P. R. Milligan, A. P. J. Luyendyk, and T. Mackey (2003), Merging airborne magnetic surveys into continental-scale compilations, *Geophysics*, *68*, 988–995.

Moritz, H. (1980), *Advanced Physical Geodesy*, Herbert Wichmann, Karlsruhe, Germany.

Paterson, N. R., and C. R. Reeves (1985), Applications of gravity and magnetic surveys: The state-of-the-art in 1985, *Geophysics*, *50*, 2558–2594.

Phillips, J. D., R. L. Reynolds, and H. Frey (1991), Crustal structure interpreted from magnetic anomalies, *Rev. Geophys.*, *29*, 416–427.

Qureshy, M. N. (1982), Geophysical and Landsat lineament mapping—An approach illustrated from west central and south India, *Photogrammetria*, *37*, 161–184.

Ravat, D., R. A. Langel, M. Purucker, J. Arkani-Hamed, and D. E. Alsdorf (1995), Global vector and scalar Magsat magnetic anomaly maps, *J. Geophys. Res.*, *100*, 20,111–20,136.

Ravat, D., K. A. Whaler, M. Pilkington, T. Sabaka, and M. Purucker (2002), Compatibility of high-altitude aeromagnetic and satellite-altitude magnetic anomalies over Canada, *Geophysics*, *67*, 546–554.

Reigber, C., H. Lühr, and P. Schwintzer (2002), CHAMP mission status, *Adv. Space Res.*, *30*, 129–134.

Socias, I., and J. Mezcua (1996), Levantamiento aeromagnetico del archipielago canario, *Publ. Tec. 35*, 28 pp., Inst. Geogr. Nacl., Madrid.

Socias, I., J. Mezcua, J. Lynam, and R. Del Potro (1991), Interpretation of an aeromagnetic survey of the Spanish mainland, *Earth Planet. Sci. Lett.*, *105*(1–3), 55–64.

Vine, F. J., and D. H. Matthews (1963), Magnetic anomalies over oceanic ridges, *Nature*, *199*, 947–949.

Wegener, A. (1912), Die Entstehung der Kontinente, *Geol. Rundsch.*, *3*, 276–292.

Wessel, P., and W. H. F. Smith (1991), Free software helps map and display data, *Eos Trans. AGU*, *72*, 441.